JOURNAL OF GEOPHYSICAL RESEARCH, VOL. 104, NO. C5, PAGES 11,049–11,064, MAY 15, 1999

Stochastically forced variability in the Antarctic Circumpolar Current

Ralf Weisse[1] and Uwe Mikolajewicz

Max-Planck-Institut für Meteorologie, Hamburg, Germany

Andreas Sterl and Sybren S. Drijfhout

Koninklijk Nederlands Meteorologisch Instituut, De Bilt, Netherlands

Abstract. Interannual fluctuations in the Antarctic Circumpolar Current (ACC) were considered. In the present study we analyze a mode of variability in the Hamburg Large-Scale Geostrophic ocean general circulation model which was driven by stochastic atmospheric forcing. The short-term atmospheric weather fluctuations were represented by a number of spatially coherent patterns of momentum, heat, and freshwater flux which were superimposed onto the climatological fluxes. These patterns were derived from an experiment with an atmospheric general circulation model forced with observed sea surface temperatures, and they were chosen randomly at each month. We found anomalies which propagate along the ACC at an interannual timescale. They can be explained by the combined effects of anomaly advection with the mean ocean circulation and integration of the short-term atmospheric weather fluctuations. Some similarities were found between our results and the concept of the Antarctic Circumpolar Wave, which was proposed recently to account for large-scale anomalies which propagate along the ACC in both the atmosphere and the ocean.

1. Introduction

Almost unaffected by continental barriers, the Antarctic Circumpolar Current (ACC) encircles the globe and forms one of the largest current systems of the world oceans. By connecting the Pacific, the Atlantic, and the Indian Ocean, the ACC enables the exchange of water masses between these three major ocean basins and plays an important role within the global ocean circulation. The ACC forms the northern boundary for the Southern Ocean, which represents an important component of the climate system. Antarctic bottom water, one of the coldest and densest water masses, is formed in the Southern Ocean. It is this water mass which cools and ventilates most of the volume of the deep oceans [e.g., *Schmitz*, 1995].

There is considerable interannual and decadal variability at high southern latitudes, and observations of sea-ice extent suggest that these features tend to propagate along the ACC [e.g., *Lemke et al.*, 1980; *Murphy et al.*, 1995]. Phase-locked anomalies of sea surface temperature (SST), sea-ice extent, sea level pressure (SLP), and meridional wind stress propagating eastward along the ACC were described by *White and Peterson* [1996] (hereinafter referred to as WP). They suggested that the anomalies circle around Antarctica in roughly 8-10 years at an average speed of 6-8 cm s^{-1}. Since the anomalies are mainly characterized by a zonal wavenumber two pattern, a timescale of 4-5 years was deduced. WP called this phenomenon the Antarctic Circumpolar Wave (ACW). The ACW was also identified by *Jacobs and Mitchell* [1996] in variations of the sea surface height in the ACC using the most recent satellite data available.

Peterson and White [1998] suggested that the ACW basically reflects a propagation of Pacific El Niño-Southern Oscillation (ENSO) signals and that the source of the interannual SST signals in the ACC is located in the western subtropical South Pacific Ocean. They concluded that ENSO-related SST anomalies propagate southward into the Southern Ocean where they move eastward, phase locked with SLP anomalies, around the entire Southern Hemisphere through some combination of geostrophic advection and atmosphere-ocean coupling.

Another mechanism which depends on strong air-sea interactions in the Southern Ocean was suggested by *Qiu and Jin* [1997]. They were looking for the normal mode solutions of a two-layer quasi-geostrophic model for the ocean coupled with an anomalous heat budget equation for the atmosphere in a zonally periodic channel. The coupling of the atmosphere and the ocean takes place via anomalous wind stresses and heat fluxes. Assuming a direct proportionality

[1]Now at GKSS-Forschungszentrum Geesthacht GmbH, Institut für Gewässerphysik, Geesthacht, Germany.

Paper number 1999JC900040.
0148-0227/99/1999JC900040$09.00

between air temperature and sea level pressure, Qiu and Jin found that the most unstable normal mode solution of their model occurred at wavenumber two and was very similar to the observed ACW. They were able to reconstruct the phase relationships among observed atmospheric and oceanic variables.

With respect to the timescale of the ACW, the period for which reliable data are available at high southern latitudes is rather limited. The validity of some of the conclusions drawn from observations must therefore be considered with care. *Christoph et al.* [1998] (hereinafter referred to as CBR) tried to find and confirm the results of WP and *Peterson and White* [1998] in a 180-year integration of a coupled atmosphere-ocean general circulation model (CGCM). They found variability strongly reminiscent of the ACW but raised some noticeable differences. In the model the turnaround time of the ACC is closer to 12-16 years compared with the 8-10 years inferred from the observations, and a wavenumber three pattern is more pronounced than a wavenumber two pattern. Additionally, CBR found noticeable regional differences in the amplitude of the variability they associated with the ACW. Compared to the Pacific, the amplitude is much smaller in the South Atlantic and Southern Indian Ocean. On the basis of these findings, they doubted that the ACW indeed circles around the globe and concluded that an equally plausible description would have the ACW appear first south of Australia, subsequently moving eastward with intensification, and immediately attenuating after passing Drake Passage. In contrast to Peterson and White, who speculated that the ACW has its source in the ENSO phenomenon, CBR argued that the mode has its origins in the midlatitudes to high latitudes themselves.

Whereas CBR considered the ACW as a phenomenon basically driven by atmospheric forcing, WP and *Qiu and Jin* [1997] concluded that the ACW is a mode of the coupled atmosphere-ocean sea-ice system and that atmosphere-ocean interaction plays a dominant role in the mechanism of the variability. The latter is a typical approach often used to explain variability of the type described above. An alternative explanation for understanding climate variability was proposed by *Hasselmann* [1976] with the concept of stochastic climate models. For timescales of a few months and longer the atmosphere is assumed to be in a quasi-equilibrium. The integration of the short-term atmospheric fluctuations transforms the essentially white-noise atmospheric forcing into a red response signal. For a linear system the resulting response spectrum is proportional to ω^{-2} as long as the frequency ω is large compared to the inverse of the natural timescale of the slow system and constant at low frequencies. This concept was successfully applied to a number of problems such as midlatitude SST variability [*Frankignoul and Reynolds*, 1983] or advection of sea ice in the Arctic and Antarctic [*Lemke et al.*, 1980].

Several extensions or generalizations of this concept have been suggested. *Griffies and Tziperman* [1995] showed an example of how white-noise atmospheric forcing may maintain a linearly damped oscillatory eigenmode in an ocean general circulation model (OGCM). *Frankignoul and Reynolds* [1983] and later *Saravanan and McWilliams* [1998] included the effect of oceanic advection and showed that preferred timescales in the slowly varying component of the system may arise, although there is no underlying oscillatory mechanism in the uncoupled ocean or the uncoupled atmosphere. Note, however, that atmosphere-ocean feedbacks are usually neglected in these concepts.

In this paper we describe and analyze a mode of interannual variability in the Southern Ocean of the Hamburg Large-Scale Geostrophic (LSG) OGCM and present a discussion in relation with the mode found by CBR in a coupled atmosphere-ocean model as well as the concept of the ACW. The mode discussed in this paper was identified in an integration in which the LSG OGCM was forced with stochastic wind stresses, heat, and freshwater fluxes superimposed on the climatological fluxes. The response to this type of forcing appears to be dominated by a strong interannual signal in the Southern Ocean, which shows substantial similarities with the mode discussed by CBR. In our experiment the signal can be explained mainly by an integration of the stochastic components of the atmospheric forcing plus ocean advection and some linear ocean feedback. Atmospheric feedbacks are neglected in our study. We suggest that the mechanism presented might be important in the real Southern Ocean.

The OGCM and the experiment are briefly described in section 2. The dominant mode of interannual variability in the Southern Ocean as it appears in the OGCM is described in section 3.1. On the basis of the concept of stochastic climate models, a simple conceptual model for the interannual variability in the ACC is presented and tested against the OGCM results in sections 3.2 and 3.3. Possible oceanic feedbacks are considered in section 3.4. Our results are summarized and discussed in section 4.

2. Model and Experiment Description

2.1. Model and Spin-Up

In the present study the Hamburg Large-Scale Geostrophic (LSG) OGCM as described by *Maier-Reimer et al.* [1993] was used. The model is based on the linearized Navier-Stokes equations, the conservation equations for heat and salt, and the equations of state [*UNESCO*, 1981] and continuity. In the latter, incompressibility is assumed. In case of vertical instability, convective adjustment is applied. The model has a free upper surface. A mass flux boundary condition is used at the sea surface. A simple sea-ice model is included. The drift velocity of sea ice consists of the ocean surface velocity plus a component proportional to the near surface wind. Furthermore, a simple runoff model is included.

The LSG OGCM is formulated on an Arakawa E-Grid [*Arakawa and Lamb*, 1977] and, in the present study, was applied with a horizontal resolution of effectively $3.5° \times 3.5°$ at 11 vertical layers, centered at 25, 75, 150, 250, 450, 700, 1000, 2000, 3000, 4000, and 5000 m depth. A realistic but smoothed topography was used, and a time step of 15 days was applied.

A model spin-up was performed for 5000 years using monthly climatologies of near-surface air temperature from the Comprehensive Ocean-Atmosphere Data Set (COADS) [*Woodruff et al.*, 1987], wind stress [*Hellerman and Rosenstein*, 1983], and the annual mean climatology of sea surface salinity [*Levitus*, 1982] until a steady state solution was obtained. Climatologies of net freshwater flux and heat flux were computed from the last 500 years of this spin-up. The model was integrated for another 4000 years using a fixed flux boundary condition for freshwater flux and a combination of a fixed flux forcing and restoring with a damping coefficient of 16 W m^{-2} K^{-1} as boundary condition for temperature [*Mikolajewicz and Maier-Reimer*, 1994].

2.2. Description of the Experiments

To account for the short-term atmospheric fluctuations which influence the ocean at its upper boundary, stochastic components were added to the climatological fluxes of momentum, freshwater, and heat. These components were derived from a 10-year Atmosphere Model Intercomparison Project (AMIP) simulation (see Appendix) with the ECHAM3-T42 atmosphere general circulation model (AGCM) [*Arpe et al.*, 1993; *Roeckner et al.*, 1992] by averaging the momentum, heat, and freshwater fluxes and the near-surface air temperature over each month and subtracting the climatology. For each month, one set of these anomalies was chosen at random and added to the climatological fluxes in the OGCM simulation. Thus the stochastic components superimposed are spatially coherent but have a white-noise spectrum with respect to time. In the absence of reliable and sufficiently resolved observational data, this spatial coherence may be regarded as a reasonable approximation for representing the spatial coherence at the synoptic scale of the atmosphere. To account for seasonal variations of the variability, only anomalies from the corresponding month of the atmospheric simulation were chosen. The model was integrated for 7000 years. However, only the last 5000 years were examined in the present study to avoid analyzing the effects of the model's adaption to the new boundary conditions. The analysis was restricted to annual mean data.

3. Interannual Variability in the Antarctic Circumpolar Current

3.1. Analysis and Description

To describe the space-time dependent variability appearing in the OGCM, we used the multivariate Principal Oscillation Pattern (POP) technique [e.g., *von Storch et al.*, 1995]. Unlike the Empirical Orthogonal Function (EOF) analysis, which is designed to yield an optimal representation of the covariance structure of the data and not to represent dynamical modes in general, the POP analysis provides a simultaneous analysis of both the spatial features (e.g., propagation) and the spectral characteristics of the data. Examples of the good agreement between the theoretical normal modes of a complex system and those estimated by a POP analysis can be found in the work of *Schnur et al.* [1993].

POPs form an eigensystem of the analyzed data $q(\vec{x}, t)$, where $\vec{x}$ is the space coordinate and t is the time coordinate,

$$q(\vec{x}, t) = \sum_i z_i(t) p_i(\vec{x}). \quad (1)$$

Here $z_i = z_{i1} + i z_{i2}$ are the complex POP-coefficient time series, and $p_i = p_{i1} + i p_{i2}$ are the spatial POP patterns. Pattern p_{i1} is referred to as the real part of the ith POP, and p_{i2} is referred to as the imaginary part of the ith POP. The system is expected to generate stochastic sequences

$$\ldots \rightarrow p_2 \rightarrow p_1 \rightarrow -p_2 \rightarrow -p_1 \rightarrow p_2 \rightarrow \ldots. \quad (2)$$

Note that the index i was dropped for convenience. Thus, if at time $t = 0$ the system is in state p_2, it will be with a high probability in state p_1 one quarter of a period later, in state $-p_2$ half a period later, and so on. The period and decay time of a POP can be deduced from its coefficient time series z. Since the POPs are normalized such that the POP-coefficient time series have unit standard deviation, the POP patterns can be interpreted as typical anomalies associated with a particular process.

We performed a POP analysis of the Southern Hemisphere sea surface salinity (SSS) as simulated in the LSG experiment. The dominant mode of variability (Figure 1) is characterized by an oscillation period and a decay time both of roughly 6 years. According to (2), the mode describes an eastward propagation of salinity anomalies along the ACC with superimposed growth and decay of anomalies. Let us consider, for example, the positive salinity anomaly southwest of Australia (Figure 1a): The anomaly moves eastward under intensification first (Figure 1b), reaches its maximum amplitude east of the dateline, and attenuates henceforth while propagating further eastward. Generally, strongest anomalies are found approximately southeast of New Zealand (typically 0.15 practical salinity units (psu)), whereas anomalies are almost negligible in the Indian Ocean. Although there are clear indications of a zonal wavenumber three pattern, the zonal variations of the amplitude of the mode can only be explained using a combination of more than only one wavenumber. We will return to this point in section 3.3.

The mode explains up to 35% of the model's total SSS variability in the ACC (Figure 1c). Locally, the explained variance is highest in the Pacific sector. The cross spectra of the POP-coefficient time series are characterized by a pronounced peak near the POP period (6 years), high coherence, and a constant phase shift of roughly 90° (Figure 2) as expected from POP theory [e.g., *von Storch et al.*, 1995].

Local values for growth and decay rates can be deduced from the geographical locations of the maxima and minima of the POP patterns [*Schnur*, 1993]. A schematic sketch obtained from such an analysis is shown in Figure 3. Three different regions can be characterized. Southwest of Australia and New Zealand, the POP describes a growth of anomalies with an increasing growth rate from west to east. In the region between 160°W and east of Drake Passage the amplitude of the POP decreases. Near Drake Passage the decay is temporally halted. In the Indian Ocean the amplitudes are

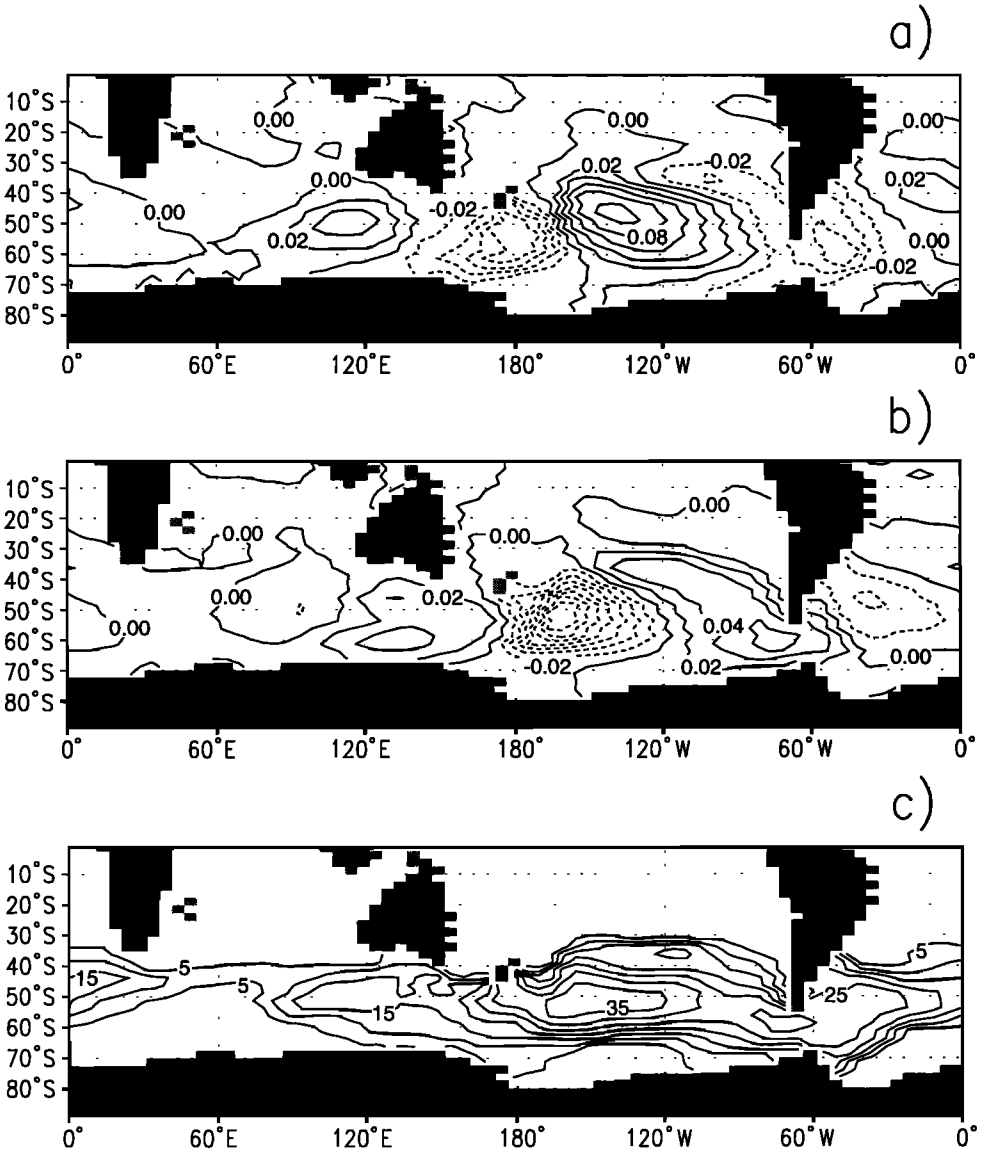

Figure 1. Spatial patterns of sea surface salinity (SSS) in practical salinity units (psu) of the dominant mode of interannual variability in the Southern Ocean: (a) imaginary part, (b) real part, and (c) locally explained variance. The contour interval is 0.02 psu for the imaginary part and the real part (Figures 1a and 1b) and 5% for the locally explained variance (Figure 1c). The model topography is shaded. Note that the model is formulated on an Arakawa E-Grid and that data and topography were transferred to a regular grid for plotting.

negligible. If we assume exponential decay and growth, we can estimate local values of e-growth and e-decay rates from Figure 3, which represent a measure for the average time it takes to increase/decrease the amplitude of SSS anomalies by a factor of e at these geographical locations. In this way we yield a growth rate of 2.2 years for the West Pacific and a decay rate of roughly 2.9 years for the East Pacific sector.

To gain insight into the way the mode is expressed in other variables of the model, associated correlation patterns of temperature and salinity at the uppermost four layers (centered at 25, 75, 150, and 250 m depth) using the POP-coefficient time series z as a bivariate index were computed. The associated correlation patterns $p_A(\vec{x})$ were derived by minimizing the expected mean squared error between some data $r(\vec{x},t)$ (e.g., temperature) and zp_A,

$$\| r(\vec{x},t) - z(t)p_A(\vec{x}) \|^2 = \min . \qquad (3)$$

Since the index is bivariate and has unit standard deviation, two patterns are obtained which can be interpreted according to (2) and which represent typical anomalies associated with the POP mode.

The associated patterns for SST also describe an eastward propagating signal (Figure 4). The strongest SST anomalies occur southeast of New Zealand and typically have values of the order of 0.35 K. However, at the sea surface the signal-to-noise ratio for temperatures is smaller compared with that for salinity. Temperature anomalies with timescales longer than the restoring timescale of 5 months are damped ow-

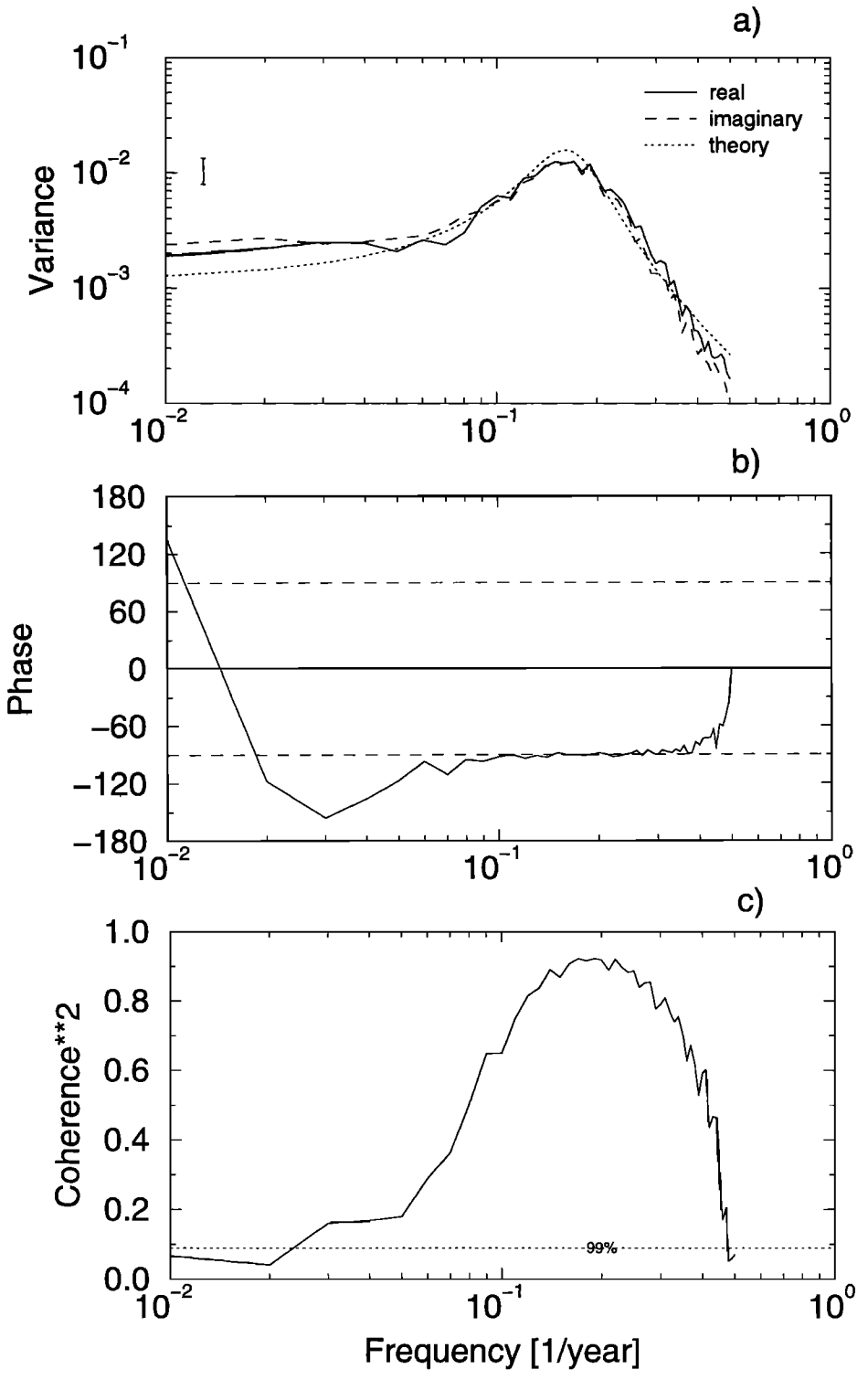

Figure 2. Spectra of the Principal Oscillation Pattern (POP)-coefficient time series of the dominant mode of interannual variability in the Antarctic Circumpolar Current (ACC): (a) power spectrum (solid line, real component; dashed line, imaginary component; dotted line, fitted theoretical model (section 3.3.3)), (b) phase spectrum, and (c) coherence squared. The bar on the left-hand side in Figure 2a represents the 95% confidence interval.

ing to the applied forcing, and the direct effect of thermal stochastic forcing leads to a higher short-term background variability. As a result, the locally explained variance is only 10-20% in the Pacific sector of the ACC. The associated patterns for temperature at 75, 150, and 250 m depth are similar to that for SST, although with a slightly larger zonal extend (not shown). The locally explained variance is somewhat larger, and typical amplitudes of the temperature anomalies are approximately 0.2 K at 150 m depth, and 0.15 K at 75, and 250 m depth (not shown).

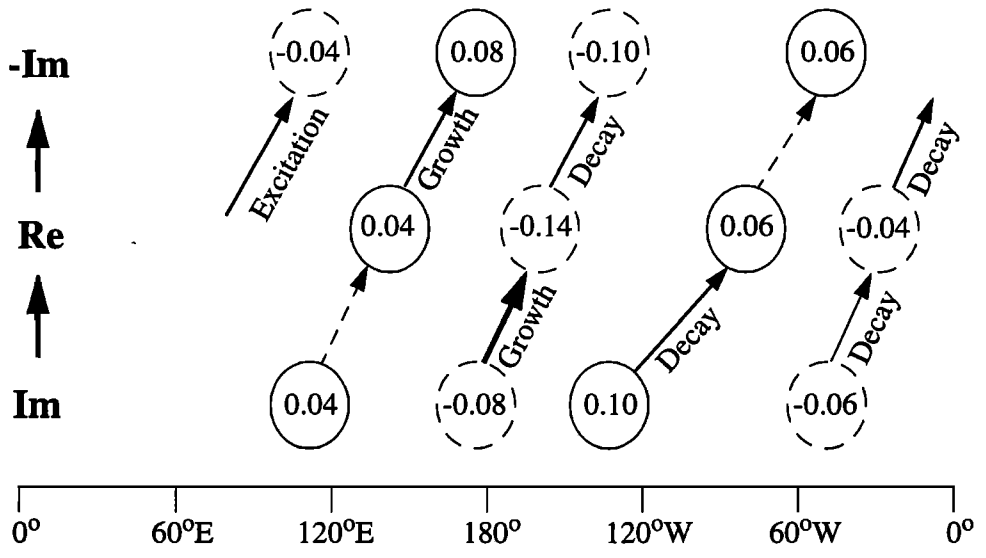

Figure 3. Schematic sketch of the dominant mode of interannual variability. Numbers denote typical amplitudes of positive (solid circles) and negative (dashed circles) salinity anomalies. The width of the arrows shows qualitatively the growth and the decay rates for the transition from the imaginary to the real and from the real to the negative of the imaginary part.

For the salinities the situation is slightly different. Here the signal is more confined to the upper two layers. At 250 m depth, anomalies of significant amplitude were only found southeast of New Zealand, where they account for roughly 25% of the local salinity variability. The restriction of the signal to a very limited region at deeper layers is probably due to the fact that anomalies here are triggered by changes in the depth of convection due to the propagating surface anomalies. These changes are strongest in regions in which the stability of the vertical stratification is small and where the surface signal is strongest (Figure 1).

The interannual variability described is to a large extent characterized by the eastward propagation of temperature and salinity anomalies. The path which the maxima of the anomalies follow coincides well with the trajectory of a passive tracer in the mean current of the model's ACC. We therefore propose that the propagation of the anomalies is basically a result of ocean advection. On the other hand, the generation of the anomalies is probably mainly a result of the integration of the stochastic atmospheric forcing. In the following we want to test the hypothesis that the interannual variability found in the LSG model can to a large extent be described as a combination of the integration of the white-noise atmospheric forcing, ocean advection, and some linear feedback. On the basis of this hypothesis, a simple conceptual model for the oceanic variability is developed in section 3.2 and compared to the results of the LSG experiment in section 3.3.

3.2. A Conceptual Model

To develop a conceptual model that incorporates the three ingredients just identified (i.e., atmospheric forcing, advection, and feedback), we consider the anomaly $q(\vec{x}, t)$ of some oceanic property like temperature or salinity. Its evolution in time can be described by the general transport equation

$$\frac{\partial q}{\partial t} + \nabla(\vec{u}q) = s, \tag{4}$$

where $\vec{u}(\vec{x}, t)$ denotes the horizontal velocity and $s(\vec{x}, t)$ denotes any source or sink of property q.

Since we consider only the horizontal transport equation, the source term includes the atmosphere-ocean fluxes as well as fluxes from below, as, for instance, the flux due to convection. Thus s is a function of low-frequency oceanic and high-frequency atmospheric variables. To separate between these two timescales, we split s into a slowly varying component $\overline{s}$ depending on the ocean conditions and a fluctuating part s' describing the influence of the atmosphere. We further assume that $\overline{s}$ can be written as a linear feedback, $\overline{s} = -\lambda q$, where λ is a constant, so that (4) becomes

$$\frac{\partial q}{\partial t} + \nabla(\vec{u}q) + \lambda q = s'. \tag{5}$$

Equation (5) is formally similar to a stochastic climate model with linear feedback and advection in which the variability of the slowly varying oceanic variable q is primarily a result of the high-frequency (atmospheric) noise forcing s'. Similar models were proposed and successfully applied, for example, to midlatitude SST variability [*Frankignoul and Reynolds,* 1983] and to the advection of sea ice in the Arctic and Antarctic [*Lemke et al.,* 1980]. It should be stressed that high-frequency oceanic variability may also contribute to s' in (5). To start with, we will test to what extent our model can explain the observed variability when s' solely consists of atmospheric fluctuations.

To further simplify the model, we assume that the anomalies are confined to a layer of constant depth, that only variations in zonal direction are important, and that advection takes place at the mean zonal velocity $\overline{u}$ of the ACC, which is assumed to be independent of space and time. With these assumptions the ACC is approximated as a straight chan-

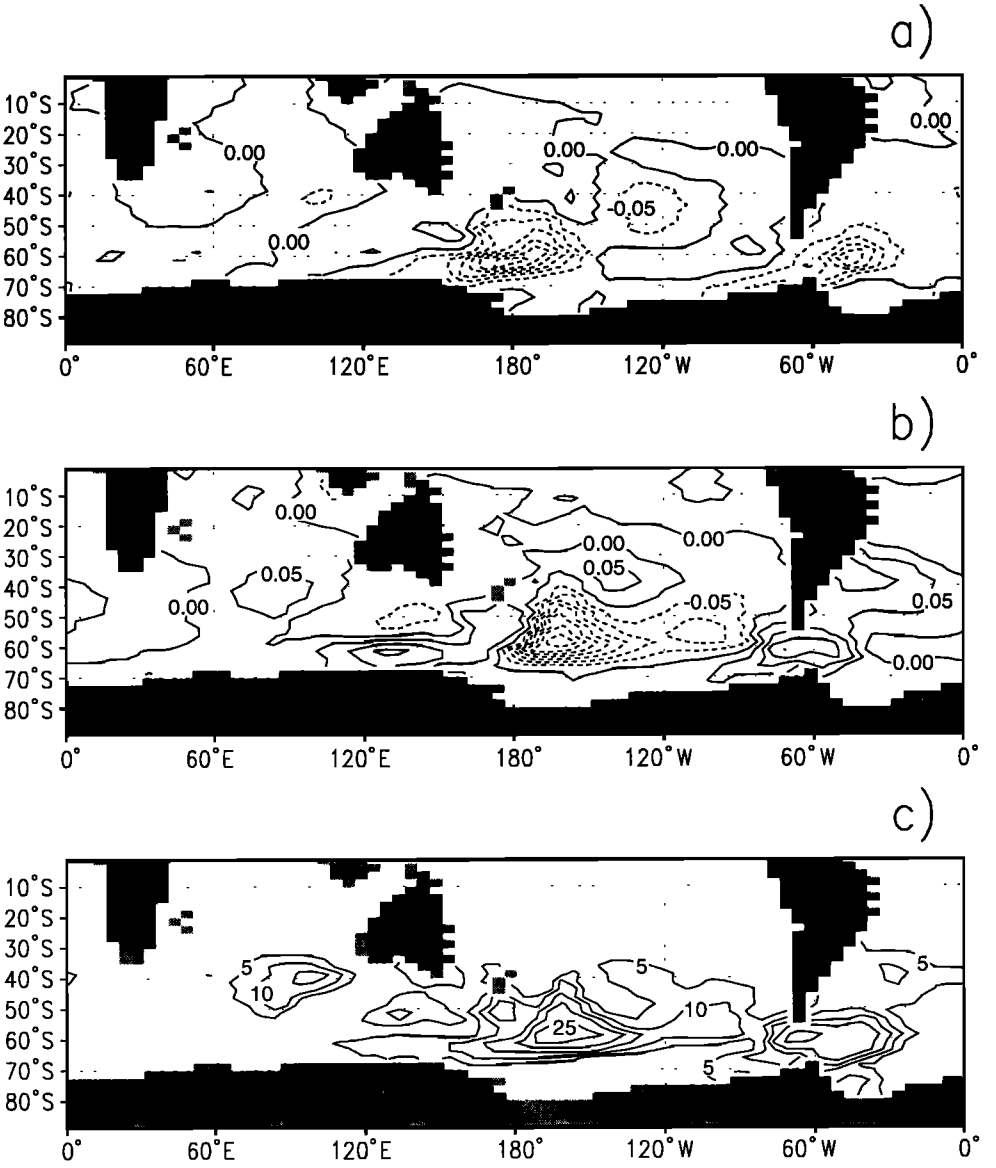

Figure 4. Associated correlation patterns of sea surface temperature (SST) in Kelvin: (a) imaginary part, (b) real part, and (c) locally explained variance. The contour interval is 0.05 K for the imaginary part and the real part (Figures 4a and 4b) and 5% for the locally explained variance (Figure 4c). The model topography is shaded. Note that the model is formulated on an Arakawa E-Grid and that data and topography were transferred to a regular grid for plotting.

nel of constant depth and width with a constant zonal flow. Equation (5) then becomes

$$\frac{\partial}{\partial t}q(x,t) + \overline{u}\frac{\partial}{\partial x}q(x,t) + \lambda q(x,t) = \nu(x,t), \qquad (6)$$

where x denotes longitude and $\nu = s'$ for later notational convenience.

To examine the spectral characteristics of our simple conceptual model, we apply Fourier transformation in space and time to (6), multiply the result with its complex conjugate, and perform ensemble averaging to yield a relation between the wavenumber-frequency (k-ω) spectrum of the atmospheric forcing $F_{\nu\nu}$ and that of the oceanic response F_{qq},

$$F_{qq}(\omega,k) = \frac{F_{\nu\nu}(\omega,k)}{(\omega - k\overline{u})^2 + \lambda^2}, \qquad (7)$$

where F_{ab} denotes the cross spectrum between a and b. In the following we use for simplification of notation within the text the dimensionless wavenumber $\tilde{k} = kR\cos\phi$, where R denotes the radius of the Earth and ϕ denotes the latitude. Within formulas, however, we retain the wavenumber k. For a white-noise atmospheric forcing, $F_{\nu\nu}$ is independent of ω. From (7) it then follows that for each wavenumber k the wavenumber-frequency spectrum F_{qq} of the ocean response has a maximum at $\omega = k\overline{u}$. In other words, in the wavenumber-frequency domain, F_{qq} peaks along a curve of constant ωk^{-1}.

For later reference we also need the variance spectrum,

which is just the wavenumber-frequency spectrum (equation (7)) integrated over all wavenumbers,

$$\hat{F}_{qq}(\omega) = \int \frac{F_{\nu\nu}(\omega, k)}{(\omega - k\overline{u})^2 + \lambda^2} dk. \quad (8)$$

The variance spectrum of the ocean response also depends on the spectrum of the forcing. If the latter is independent of ω (i.e., white noise) but has a distinct maximum at a certain wavenumber k_0, the variance spectrum (equation (8)) will have a peak at frequency $k_0\overline{u}$. In this case the spatial coherence of the forcing is mapped onto the slow system and determines the timescale T of the oceanic response through $T = 2\pi(k_0\overline{u})^{-1}$.

A similar model was presented and discussed by *Saravanan and McWilliams* [1998], who investigated interannual and decadal variability in the North Atlantic region. They arrived at an equation similar to (6) (their equations 9 and 10) and found that their model can give rise to a preferred timescale $T = L/V$, where the length scale L is associated with the atmospheric variability and the velocity scale V is associated with the advection in the upper ocean. The timescale L/V of Saravanan and McWilliams is identical to the timescale $T = 2\pi(k_0\overline{u})^{-1}$ of our conceptual model.

3.3. Model Testing

In section 3.2 we derived a simple model (equation (6)) to describe the generation and propagation of anomalies in the Southern Ocean. We are now going to test whether this model is consistent with the main results from the LSG model as discussed in section 3.1.

3.3.1. Wavenumber-frequency spectra. We compared the wavenumber-frequency spectra calculated from the LSG experiment data with those predicted by our conceptual model (equation (7)). For this purpose we expanded temperature and salinity at 51°S and 61°S at the sea surface and at 75 m depth into a series of sine and cosine functions along each latitude belt. The time dependent sine and cosine coefficients $b_k(t)$ and $a_k(t)$ are assumed to be a random realization of a bivariate stochastic process and are used to estimate the wavenumber-frequency spectrum given by

$$F_{ab}(\omega, k) = \frac{1}{2}[F_{aa} + F_{bb}](\omega, k) - Q_{ab}(\omega, k), \quad (9)$$

where Q_{ab} represents the quadrature spectrum of the sine and cosine coefficients [*von Storch and Zwiers*, 1999]. Additional heuristic arguments are used to assign parts of the overall variance to standing and propagating waves. We use the definition of *Pratt* [1976], who interprets the minimum of westward and eastward propagating variance as standing variance and labels the remainder as propagating variance. With this interpretation the standing variance comprises all standing plus all random fluctuations.

A large fraction of the SSS variance at 51°S is accounted for by a standing wavenumber one pattern with a timescale of 40 to 50 years (Figure 5b). Near the POP period of 6 years, most of the SSS variance is attributed to the propagating part of the spectrum at zonal wavenumbers 1-3 (Figure 5a). In accordance with the spectrum of our conceptual model (equation (7)), the maximum of the propagating variance is centered along a curve of almost constant ωk^{-1}: For $\tilde{k} = 1$ the maximum variance occurs at a period of roughly 18 years, for $\tilde{k} = 2$ it occurs at a period of roughly 9 years, and for $\tilde{k} = 3$ it occurs at roughly 6 years, resulting in a propagation speed of 20° yr^{-1}. Using a mean radius of the Earth of 6370 km, this is equivalent to an average propagation speed of 4.4 cm s^{-1} at 51°S.

We compared this velocity to the zonally and vertically averaged velocity in the LSG model (Figure 6). In the Southern Hemisphere the largest velocities occur approximately in the latitude belt between 40°S and 50°S (Figure 6a). The exact value of the maximum zonally averaged zonal velocity depends on the range over which the depth average is taken (Figure 6b). Within the surface layer the largest velocity is 4.56 cm s^{-1}. If we average over the top two layers, the maximum velocity yields 4.24 cm s^{-1}. When averaging is performed over the uppermost four layers, this velocity decreases down to 3.54 cm s^{-1}. Since the interannual mode described above is basically a surface phenomenon, the propagation speed of the anomalies derived from the wavenumber-frequency spectrum is a plausible advection speed due to the modeled ACC.

Similar conclusions as those for SSS hold for the wavenumber-frequency spectra of SST and of temperature and salinity at 75 m depth at 51°S and 61°S. These spectra are similar to that of SSS, however, with a smaller signal-to-noise ratio (not shown). The wavenumber-frequency spectra for temperature and salinity estimated from the LSG experiment data are thus in accordance with those predicted by our conceptual model (equation (7)). The propagation speed of the anomalies is in accordance with a rough estimate of the mean velocity of the ACC in our OGCM.

3.3.2. Spatial forcing patterns. At the end of section 3.2 we discussed the possibility that if most of the atmospheric variability could be attributed to only a few wavenumbers, this may, together with a characteristic velocity scale in the ocean, determine the timescale of the ocean response. To test this hypothesis we used (9) to estimate the wavenumber-frequency spectra of all atmospheric forcing components (boundary temperature, net freshwater flux, and wind stress curl) used in the LSG experiment. Most of the variance in these spectra is attributed to wavenumbers 1-3, depending on the component of the forcing (Figure 7). This supports our conceptual model (equation (6)), as a combination of more than one dominant wavenumber in the forcing fields is necessary to account for the zonal modifications of the amplitude of the ocean response as found for the POP mode (Figure 1). We will discuss this in more detail in section 3.3.4.

With respect to frequency the wavenumber-frequency spectra are almost constant. This is typical for white-noise processes. The variance of the model forcing which is attributed to the standing part of the spectrum is usually 1-2 orders of magnitude larger than that associated with the propagating part. This results from the fact that the atmospheric forcing of the LSG experiment consists of a limited

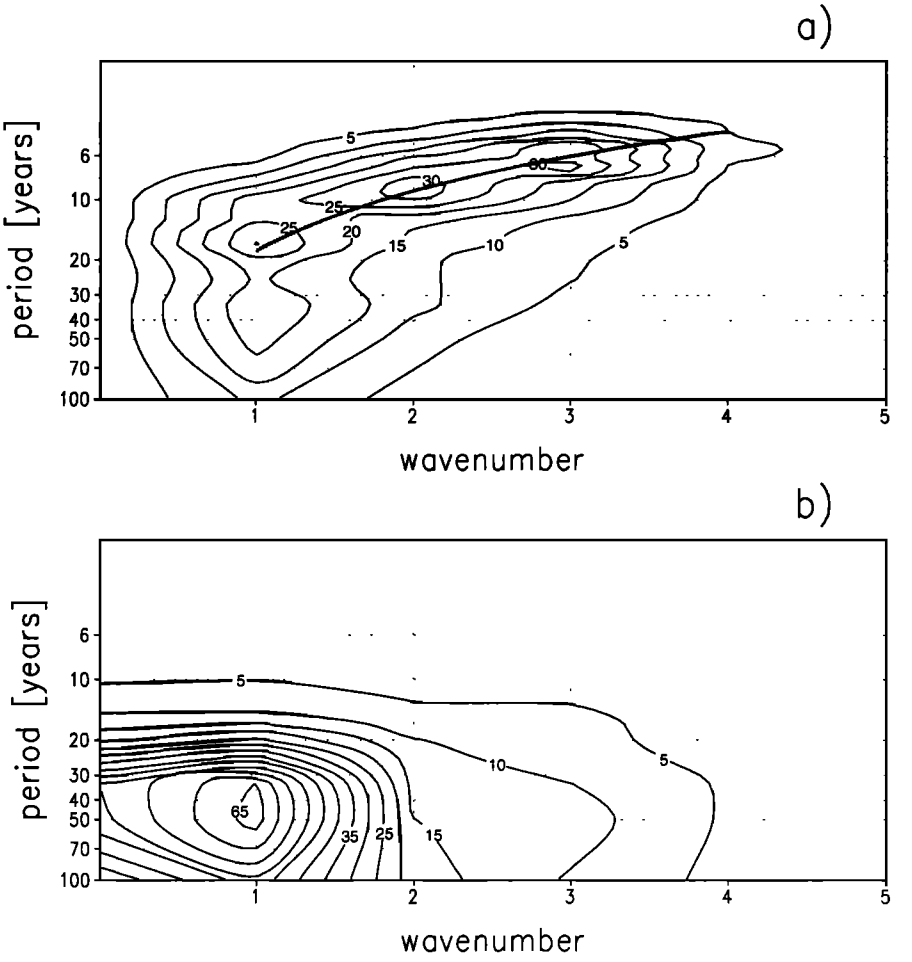

Figure 5. Two-sided wavenumber-frequency spectrum of the SSS at 51°S in 10^{-5} psu^2 $\Delta\omega^{-1}$ Δk^{-1}: (a) propagating variance and (b) standing variance. In Figure 5a the curve $T\tilde{k} = 18$ years is indicated by the bold line. It corresponds to a curve of constant advection velocity of $2\pi R\cos(\phi)(T\tilde{k})^{-1} = 4.4$ cm s^{-1}.

number of spatial patterns which were chosen randomly in time. Thus there is no preferred propagation direction, and the variance is dominated by the standing part of the spectrum. Therefore only the total variance is shown in Figure 7.

Although we cannot draw any conclusions from the relative amount of atmospheric variance explained by the propagating and the standing part of the spectrum in our experiment, there is some observational evidence that the chosen forcing nevertheless represents an adequate approximation of the real situation. For instance, *Mo and White* [1985] and *Xu et al.* [1990] report a preference of the atmosphere to attribute energy to the standing part of the spectrum in the midlatitudes of the Southern Hemisphere. *Connolley* [1997] reached similar conclusions and suggested that the patterns of the atmospheric variability at high southern latitudes are a characteristic of the land-sea distribution and the topography.

3.3.3. Model fit. As shown in sections 3.3.1 and 3.3.2, there is general agreement between the wavenumber-frequency spectra derived from our conceptual model (equation (6)) and those of the atmospheric forcing and the ocean response in the LSG experiment. We now apply our conceptual model to the POP-coefficient time series. To check if both spectra are consistent, we fitted the spectrum (equation (8)) of our conceptual model to the spectra of the POP-coefficient time series. For simplicity, we assumed that the white-noise atmospheric forcing $F_{\nu\nu}(\omega, k)$ is dominated by a wavenumber three pattern. Then (8) reduces to

$$\hat{F}_{qq}(\omega) = \frac{A_{\nu\nu}}{(\omega - k_0\overline{u})^2 + \lambda^2}, \tag{10}$$

where $\tilde{k_0} = 3$ and $A_{\nu\nu} = F_{\nu\nu}(0, \tilde{k_0} = 3)$ is the constant amplitude of the stochastic forcing. Fitting (10) to the spectrum of the POP-coefficient time series, a good agreement was obtained (Figure 2a). The model parameters $A_{\nu\nu}$, $\overline{u}$, and λ were estimated by a least squares fit, minimizing the deviation between the power spectra of the POP coefficients and the conceptual model. In this way we obtained a mean velocity of roughly 0.342 rad yr^{-1}, which is equivalent to almost 20° yr^{-1}, or 4.4 cm s^{-1} at 51°S. It coincides with the vertically and zonally averaged zonal velocity between 40°S and 50°S (Figure 6), which is a rough approximation of the average speed of the ACC in the LSG model. Additionally, a turnaround time around Antarctica of roughly 19 years can be inferred. Because of the assumed wavenumber three pat-

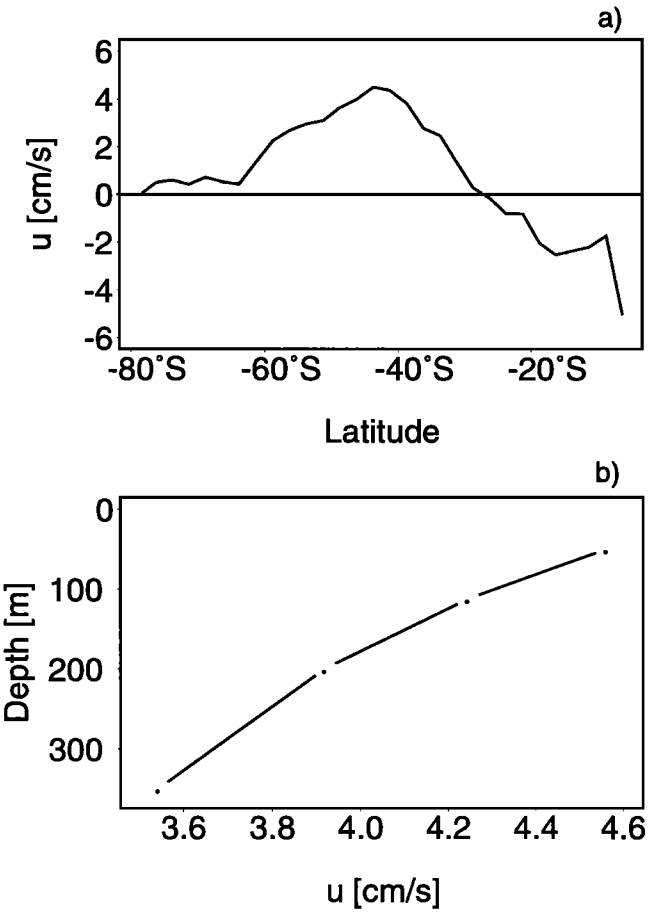

Figure 6. (a) Mean zonally averaged zonal velocity in the surface layer in cm s^{-1} as a function of latitude. (b) Maximum mean zonally and vertically averaged zonal velocity between 40°S and 50°S in cm s^{-1} as function of depth. Depth averaging was performed from the surface down to the depth given at the ordinate.

tern in the atmospheric forcing ($\tilde{k_0} = 3$), this corresponds to a characteristic timescale $T = 2\pi R\cos(\phi)(\tilde{k_0}\overline{u})^{-1}$ of roughly 6 years, coinciding with the estimated POP period. The feedback term λ yields 0.28 yr^{-1}, corresponding to an e-folding time of almost 4 years. The white-noise forcing level was estimated to be 1.239×10^{-3} yr^{-1}. Note that POP-coefficient time series are dimensionless in our case.

3.3.4. Characteristics of the discretized conceptual model. To demonstrate that the qualitative characteristics of our conceptual model match those of the interannual mode of variability in the ACC of the LSG model, the discretized version of (6) was adopted to temperature anomalies T,

$$\frac{T_{x,t+1} - T_{x,t}}{\Delta t} + \overline{u}\frac{T_{x+1,t} - T_{x,t}}{\Delta x} + \frac{\kappa}{c_p \rho \Delta z} T_{x,t} = \frac{\nu_{x,t}}{c_p \rho \Delta z}, \tag{11}$$

and integrated forward in time for 100 years. Here x denotes longitude, t denotes time, $c_p = 3994$ J kg^{-1} K^{-1} is the specific heat of sea water at constant pressure, and $\rho = 1000$ kg m^{-3} is the density of sea water. The ratio of the damping factor κ and the surface layer thickness Δz was chosen to be 3.6×10^{-2} W m^{-3} K^{-1}, corresponding to a linear feedback of $\lambda = 0.28$ yr^{-1} as estimated from the POP coefficients. The average velocity $\overline{u}$ was set to 4.5 cm s^{-1}, an approximation of the mean velocity of the ACC in the LSG OGCM. For the zonal resolution Δx we choose roughly 350 km, which corresponds to 72 grid points at 51°S, and for the time step Δt we choose one month. The white-noise forcing function ν was represented by

$$\nu(x,t) = A_1(t)\cos[k_1 x + \phi_1(t)] + A_2(t)\cos[k_2 x + \phi_2(t)], \tag{12}$$

where k_i denotes wavenumber, ϕ_i denotes phase, and A_i denotes the amplitude of the forcing.

Three different experiments were carried out. In the first experiment (E1) merely a wavenumber three forcing was used ($\tilde{k_1} = 3$ and $A_2(t) = \phi_1(t) = \phi_2(t) = 0$), and the amplitude $A_1(t)$ was chosen randomly with respect to time. In the second experiment (E2) we used a superposition of wavenumbers two and three ($\tilde{k_1} = 3$ and $\tilde{k_2} = 2$) with a common but randomly chosen amplitude ($A_1(t) = A_2(t)$) and constant phase ($\phi_1 = \phi_2 = 0$). The third experiment (E3) is similar to E2, except that all amplitudes and phases are uncorrelated and vary independently with time, such that there is no constant phase relationship among both components of the forcing.

Figure 8 shows Hovmoeller diagrams for the temperature anomalies in all three experiments. In all cases there are clear indications of anomalies propagating at the mean current velocity, yielding a turnaround time of 18 years. If the variance of the forcing is dominated by only one wavenumber (E1), no zonal modifications of the amplitude of the ocean response are found (Figure 8a). However, if a combination of at least two wavenumbers with a fixed phase relationship is chosen (E2), remarkable zonal amplitude modifications are obtained (Figure 8b). If the constant phase constraint is relaxed (E3), no clear zonal modification of the amplitude of the response emerges (Figure 8c). Therefore a fixed spatial phase of at least two different wavenumbers of the forcing is a necessary prerequisite for the zonal variations of the ocean response to be explicable in terms of our conceptual model, i.e., in terms of the atmospheric forcing. The fixed spatial phase results in zonal variations of the mean amplitude of the stochastic forcing. An analysis of the atmospheric forcing fields used in our OGCM experiment indeed shows that their amplitudes are generally larger in the Pacific than in the Atlantic and the Indic sector of the ACC (not shown).

Concluding, there is noticeable agreement between the variability in the LSG model as described by the POP mode and the results obtained with the proposed simple conceptual model (6). A combination of the integration of the white-noise atmospheric forcing, ocean advection, and some linear feedback seems plausible and is sufficient to describe the interannual variability simulated in the LSG model at a first-order approximation.

3.4. Ocean Feedbacks

Up to now we assumed an essentially passive ocean in formulating our conceptual model to explain the interannual variability found in the ACC of our stochastically forced

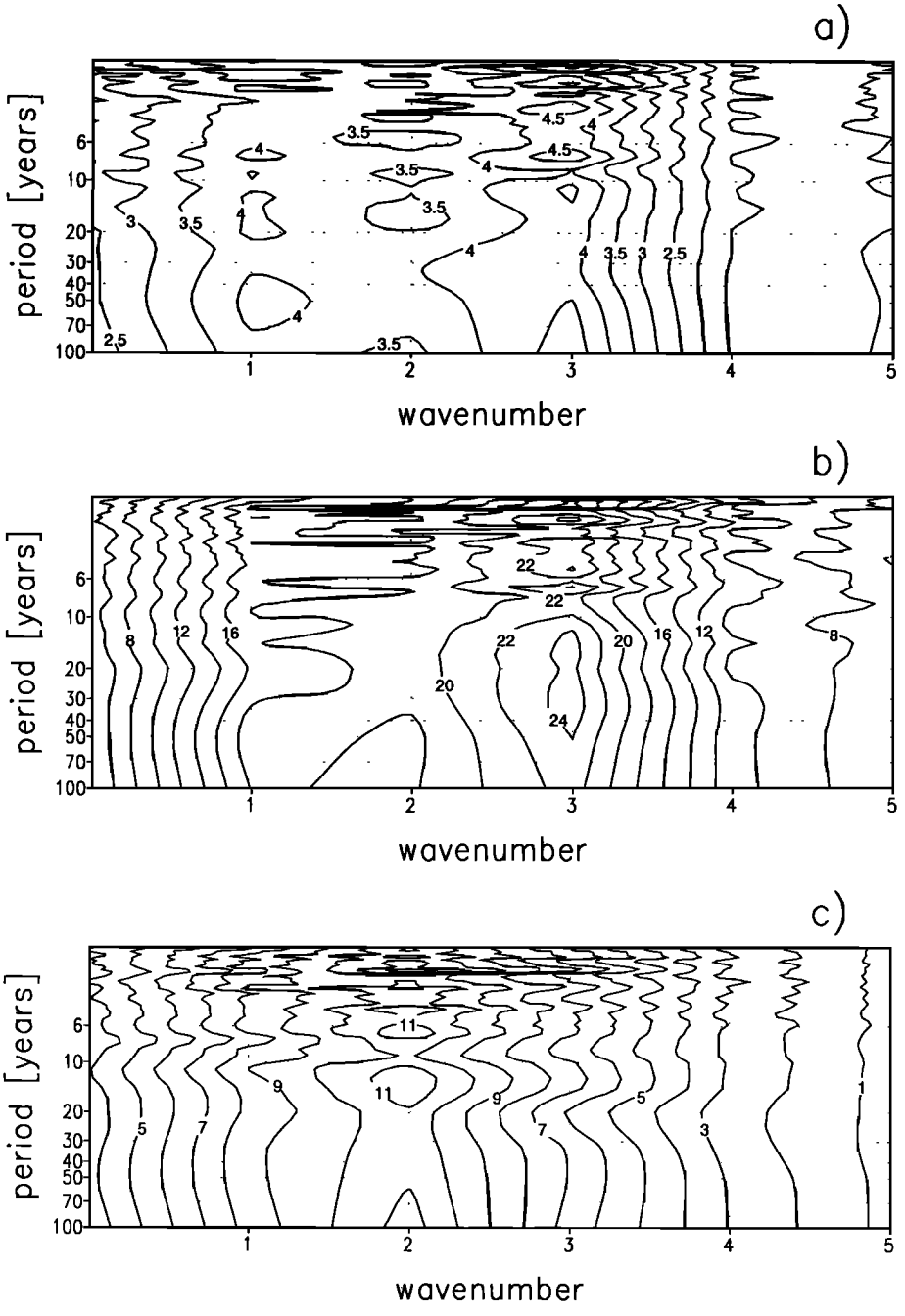

Figure 7. One-sided wavenumber-frequency spectra of the atmospheric forcing at 51°S: (a) wind stress curl, (b) freshwater flux, and (c) boundary temperature. Units are 10^{-12} Pa^2 m^{-1} $\Delta\omega^{-1}$ Δk^{-1} for Figure 7a, 10^{-12} (millimeters per month)^2 $\Delta\omega^{-1}$ Δk^{-1} for Figure 7b and 10^{-5} K^2 $\Delta\omega^{-1}$ Δk^{-1} for Figure 7c.

OGCM experiment. However, indications do exist that positive feedbacks might significantly contribute to the observed variability. For instance, we found a stronger damping of the anomalies in the Indian Ocean and East Atlantic as compared with the Pacific. In our case the most prominent candidate for positive oceanic feedbacks is oceanic convection.

The relevance of convective feedbacks for the described mode of interannual variability in the ACC of the LSG model is indicated by the change of sign of the anomalies of the associated correlation patterns at a depth between 75 and 150 m, depending on location. As cold and fresh water overlies warmer and saltier water in the upper Southern Ocean, there exist many regions where the stratification is only marginally stable and where positive SSS anomalies may trigger deeper convection in winter, which in turn leads to an amplification of the salinity anomalies at the sea surface owing to enhanced mixing with saltier water from below. Similarly, negative SSS anomalies can be amplified by reduced convection and reduced mixing with the underlying saltier water.

To assess locally the relative importance of stochastic forcing and convective feedbacks, we computed the asso-

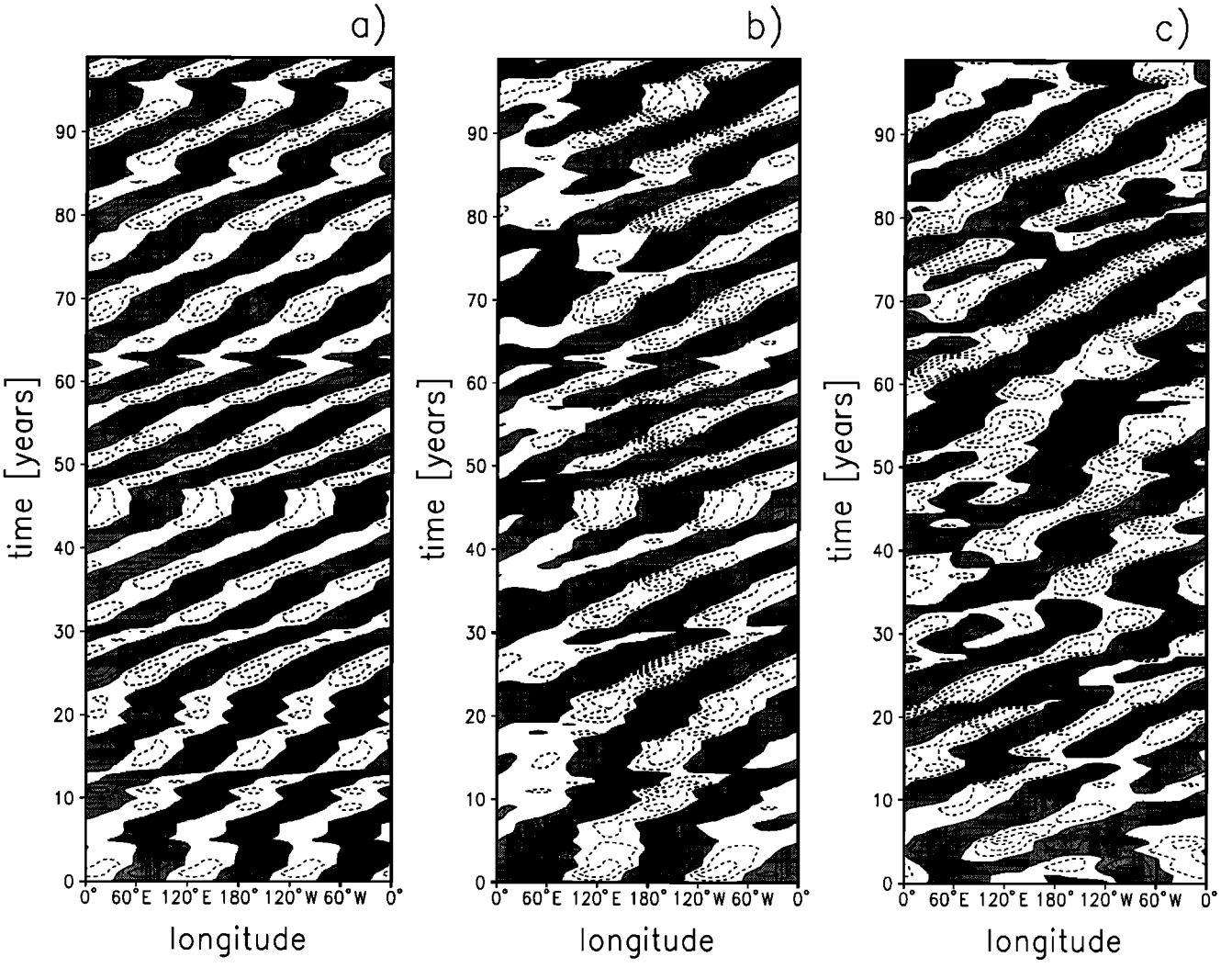

Figure 8. Hovmoeller diagrams of simulated SST response at 51°S using a simple one-dimensional model of the ACC with (a) randomly forced wavenumber three atmospheric patterns, (b) a superposition of randomly forced and spatially fixed wavenumber two and three atmospheric patterns, and (c) a superposition of randomly forced and spatially uncorrelated wavenumber two and three atmospheric patterns. Contour interval is 0.04 K. Isolines with negative values are dashed. Areas with positive values are shaded. Transition between white and shaded areas marks the zero line. Note that the longitude is artificial.

ciated correlation patterns $p_A(\vec{x}, z)$ of the salinity at all layers, again using the POP-coefficient time series as a bivariate index (equation (3)). Here z denotes depth. From these patterns we computed the anomalous salt content in a water column $S(\vec{x}, z_k)$ by

$$S(\vec{x}, z_k) = \sum_{i=1}^{k} p_A(\vec{x}, z_i)\Delta z_i, \qquad (13)$$

where z_1 represents the sea surface (the uppermost layer) and Δz_i denotes the thickness of layer i. There are no atmospheric feedbacks for the SSS. Convection can only vertically redistribute the salt. Hence a positive salinity anomaly at the sea surface due to anomalous convection must be balanced by negative anomalies at depth and vice versa. In this case the integral (13) over the entire water column yields zero. All deviations of (13) from zero show the direct effect of the stochastic forcing, either as direct integration of anomalous freshwater fluxes or as the effect of anomalous horizontal salt transports. The latter can originate, for instance, directly from anomalous Ekman transports or from the interaction of existing anomalies with a vertically sheared flow field.

Thus the ratio between the anomalous salt content in the near-surface layers (which is a measure of the signal strength) and the asymptotic value at depth gives an estimate of the relative importance of local vertical redistribution processes (e.g., convection) compared to direct integration of the forcing and horizontal exchange processes. In the regions where the mode has large amplitudes (especially in the South Pacific), we found that (13) reaches a maximum at typically 75 m depth (starting from the sea surface), before it reaches a deep saturation value. In general, the changes below 450 m are small and will be neglected here. In the region between 170°E and 150°W in the latitude belt between 40°S and 60° S, the anomalous salt content of the upper 113 m is typically more than twice as large as the total vertically integrated anomalous salt content integrated over the entire

water column. This is the region where the mode has the highest amplitudes in surface salinity. Here the anomalies generally change the sign at depths between 75 and 150 m. Our analysis reveals that in this region, local convection significantly contributes to the amplitudes of the SSS anomalies as obtained from our POP analysis. In all other regions, local convection has a smaller influence on the SSS anomalies compared to other processes like stochastic forcing.

Experiments in which various types of forcing were switched on and off did not lead to the identification of a single type of forcing that is responsible for the generation of salinity anomalies in the Southern Ocean. It appears that both heat flux and wind stress are important, with the latter slightly dominating, while freshwater flux forcing seems to play a minor role, which is consistent with the findings in a recent paper by *Bonekamp et al.* [1999]. The importance of wind stress implies that modes of variability with strong signatures in the temperature and salinity structure can also be induced by stochastically varying Ekman transports. The ability to generate the mode described in the present paper with significant amplitude with the stochastic forcing restricted to heat flux variations shows that anomalous convection (triggered by anomalous heat fluxes) in connection with a vertical shear of the horizontal velocities also contributes considerably to the excitation of this mode.

As an additional test, we performed an experiment which was identical to the one described in section 2.2 but with convection shut off. As expected, the model climate immediately started to drift strongly when convection was shut off. Whereas the length scale of the forcing remains constant, the advective velocity scale (average ACC speed) changes but not an order of magnitude. The depth scale over which the forcing is distributed, however, as well as the background climate including the subsurface temperature and salinity gradients are strongly affected by the switched off convective adjustment algorithm. The results of this experiment show that the interannual variability in the ACC decreases by a factor of 3. However, the spatial pattern of the variability remains nearly unchanged. This implies that the "passive ocean" stochastic theory can give a first-order explanation of the interannual variability found in the ACC of the LSG model. However, the amplitude is partially determined by convective feedbacks. A direct translation of the amount of reduction in the amplitude of the mode into a measure of the relative importance of convective feedbacks is not justified owing to the potential effect of the model drift on the stability characteristics and patterns of the eigenmodes of the model. Beside this, convection is likely to be the most important mechanism that creates salinity anomalies by anomalous convection as model response to heat flux anomalies. We may only conclude that convective feedbacks exist and that they are potentially important in the Western Pacific sector of the ACC. This supports our findings from the analysis of the anomalous salt content.

4. Summary and Discussion

The Hamburg LSG OGCM was forced with stochastic components added to the climatological fluxes of momentum, heat, and freshwater. In the Southern Ocean, pronounced interannual variability was excited. It is characterized by salinity and temperature anomalies in the upper levels, which propagate eastward along the ACC at the mean current velocity. The amplitude of the anomalies is at maximum in the Pacific sector of the ACC and almost negligible in the Indian Ocean. The mode was identified by means of a POP analysis of sea surface salinities for which it locally explains up to 35% of the total variance. POP analysis reveals that the anomalies are enforced or generated southwest of Australia and New Zealand. Subsequently, they are advected through the Pacific sector of the ACC and are decaying in the East Pacific, and after having passed through Drake Passage. The timescale of the variability was found to be 6 years.

The spectra of the POP coefficients coincide well with the theoretical spectrum of a stochastic climate model with linear feedback and advection in which the ocean acts primarily as integrator of the short-term atmospheric fluctuations and transfers them into a red response signal. For a given timescale of the variability of roughly 6 years (the POP period), the agreement between the spectrum of the stochastic climate model and those of the POP coefficients is best for a characteristic length scale of the atmospheric forcing patterns, which corresponds to a zonal wavenumber pattern $\tilde{k}_0 = 3$, and a mean zonal velocity at which the anomalies in the ocean are advected of $\overline{u} = 4.4$ cm s^{-1}. These values correspond to the characteristic length scale of the fixed spatial atmospheric patterns which were used to force the LSG model and the vertically and zonally averaged zonal velocity between 40°S and 50°S. The latter can be considered as an estimate of the average speed of the ACC in the LSG model. Other combinations of k_0 and $\overline{u}$, which would yield equally good agreements between the theoretical spectrum of the stochastic climate model and those of the POP coefficients, are physically less plausible and are not confirmed by our analyses.

Two properties of the atmospheric forcing were found to be important for the interannual ocean variability diagnosed in our OGCM experiment to be explicable in terms of that forcing: the characteristic length scale of the forcing patterns and their stochastic behavior in time, which, in our experiment, is fulfilled by representing the short-term atmospheric weather fluctuations by a number of spatially fixed and coherent patterns of momentum, heat, and freshwater flux which were chosen randomly with respect to time. Some support can be found that this type of forcing represents a first-order approximation of the situation found in the real Southern Ocean: *Connolley* [1997] showed that the temporal variability in the mean sea level pressure (MSLP) south of 40°S is characterized by a "white" spectrum, which is consistent with "random" forcing by weather events and a "decoupling" ocean integration. He further found that the spatial pattern of MSLP variability shows a large-scale structure that is consistent between observations and various models, and he suggested that the pattern of variability is a characteristic of the land-sea distribution and topography. His findings are supported by the earlier analyses of *Mo and White* [1985] and *Xu et al.* [1990], who showed

that a preference of the atmosphere to attribute energy to the zonal wavenumber three in the standing part of the spectrum in midlatitudes of the Southern Hemisphere does exist.

The spatial patterns of the short-term atmospheric weather fluctuations used to force the LSG OGCM in our experiment were obtained from an atmospheric GCM forced with observed SSTs. The probability that the characteristic length scale of these forcing patterns might be simply a result of the response of the atmospheric GCM to the prescribed SSTs appears to be small: Several authors provided evidence that at the interannual timescale the dominant forcing at high southern latitudes is atmosphere to ocean and that the feedback of SST anomalies on the atmospheric circulation is relatively small. *Basher and Thompson* [1996] found that SSTs in the New Zealand region lagged air temperature anomalies by half a month, which indicates that the dominant forcing is atmosphere to ocean at high southern latitudes. *Rowell* [1998] investigated an ensemble of six atmosphere model integrations forced with observed SST and sea ice starting from modified initial conditions. He found that the SST forcing has a strong direct effect in the tropics and only little direct effect in the midlatitudes to high latitudes except in spring in the far southeast Pacific. *Connolley* [1997] used a hierarchy of climate models (uncoupled atmosphere model forced with climatological SST, uncoupled atmosphere model forced with observed SST (AMIP style), and coupled atmosphere-ocean model experiments) together with observations. He showed that although an increase in atmospheric variability is seen within the hierarchy of model runs, even an uncoupled atmospheric model without interannual variations in the SST captures most of the observed atmospheric interannual variability, and he concluded that the models are sufficiently skillful to reproduce the patterns of observed variability. However, it should be emphasized that there is still ongoing discussion on atmosphere-ocean interaction at midlatitudes to high latitudes.

We conclude that the variability occurring in the ACC in our LSG experiment can to a good level of approximation be described by our proposed conceptual stochastic model. In this model, it is the large-scale spatial coherence of the atmospheric forcing which is transferred to the ocean and which together with the average zonal velocity of the ACC determines the timescale of the oceanic variability. This is the same mechanism as described by *Saravanan and McWilliams* [1998], who elaborated the role of atmospheric teleconnections in stochastically forcing extratropical ocean variability. They noted that atmospheric variability on timescales of a month and longer is dominated by a few large-scale spatial patterns, whose time evolution has a significant stochastic component. These teleconnections imprint their patterns onto the ocean through the associated flux exchange, possibly modified by ocean advection. As in our model, a spectral peak arises at the timescale set by the ratio of the length scale of the forcing to the advective velocity scale in the ocean. In this theory the ocean essentially plays a passive role; no oscillatory modes are required to explain a preferred timescale of the oceanic variability.

There are strong similarities between the interannual variability found in the Southern Ocean of the LSG model and that described by CBR for a CGCM. CBR associated this variability with the Antarctic Circumpolar Wave as described by WP. A typical amplitude of the mode of CBR is roughly 0.1-0.2 K, which is consistent with the typical strength of a SST anomaly associated with the mode in our ocean-only experiment which is roughly 0.35 K (Figure 4). Thus the magnitudes of both modes are comparable. If we suppose that both modes represent the same physical phenomenon, this indicates that stochastic atmospheric forcing is a first-order process for the excitation of the described mode, while atmosphere-ocean feedbacks play a minor role. This corresponds with the findings of CBR, who considered their mode as a phenomenon basically driven by atmospheric forcing.

CBR further emphasized that their mode is basically confined to the Pacific sector of the ACC and that its amplitude is much weaker in the Atlantic and the Indian Ocean. Furthermore, they pointed out that in their model the patterns for SLP and meridional wind stress seem to be governed by standing oscillations. They argued that the discrepancies between their results and those of WP might be partly an artifact of the short observational data records. Coinciding with the findings of CBR, the amplitude of the mode in our ocean-only experiment, in which atmosphere-ocean feedbacks are completely neglected, is at maximum in the Pacific sector of the ACC and almost negligible in the Indian Ocean. However, since we found the spatial characteristics of the atmospheric forcing to be important for the temporal and the spatial scale of the oceanic variability in our experiment, our findings cannot be considered as completely independent of those of CBR: The atmospheric part of their CGCM is almost the same as the one used for the AMIP simulation [*Arpe et al.*, 1993] from which the stochastic forcing of the LSG experiment in the present study was derived.

CBR concluded that the propagating oceanic anomalies interact with a spatially fixed resonant atmospheric background pattern such that the oceanic anomalies are selectively amplified or dissipated. They forced a simple one-dimensional ocean heat budget model for the ACC with a standing wave given by a spatially fixed wavenumber three and an oscillation period of 4 years. They were able to excite SST anomalies with a zonal wavenumber three distribution which propagate eastward along the ACC. However, no explanation was given where the 4-year period of the atmospheric fluctuations might come from. In contrast, we found that even a stochastic atmospheric forcing is able to generate an organized oceanic response which shows noticeable similarities with the variability described by CBR. By using a similar simple model, we showed in the present study that irregular atmospheric fluctuations in time are sufficient to excite propagating signals in the SST or SSS. With a spatially fixed zonal wavenumber three pattern, we were able to reconstruct basic features of the variability in the ACC such as the spatial scale of the ocean response or the propagation of the anomalies at the mean velocity of the ACC. With a combination of spatially fixed wavenumber three and two patterns as suggested by the results of our wavenumber-

frequency analysis of the atmospheric forcing, we were also able to reconstruct the zonal modifications of the amplitude of the interannual variability. In our conceptual model no preferred timescales of the atmospheric forcing are required to explain a preferred timescale of the oceanic variability: A spectral peak of the ocean response arises at the timescale set by the ratio of the length scale of the forcing and the advective velocity scale in the ocean. The ocean essentially plays a passive role. In our experiments the spatial patterns of the forcing were chosen randomly in time from an AMIP-style AGCM experiment. As a result, the variability of the forcing is dominated by standing waves. These waves have essentially similar patterns and amplitudes in observations, coupled GCMs, uncoupled GCMs, and AMIP-style integrations of atmospheric GCMs [e.g., *Conolley*, 1997; *Xu et al.*, 1990; *Mo and White*, 1985].

Compared to the ACW as described by WP from observations, the mode of variability presented in this paper shows similarities and differences: The observed ACW may have a slightly larger amplitude than the modeled mode. Within the band-pass filtered observations, WP found typical values of SST anomalies of 0.5 K, whereas typical amplitudes of our mode are 0.35 K. Another difference between observed and modeled SST anomalies lies in the zonal modification of the strength of the SST anomalies. Analyzing observations, WP suggested that phase-locked anomalies of SST, SLP, and mean meridional wind stress completely circle around the globe, and they concluded that the ACW reflects a coupled mode of the atmosphere-ocean system. Our modeled mode is basically confined to the Pacific sector of the ACC. It is much weaker in the Atlantic and the Indian Ocean, and atmospheric feedbacks are completely neglected in our study. From observations, WP estimated an ACW propagation speed of 6-8 cm s^{-1}. In our modeled mode the anomalies propagate at 4.4 cm s^{-1} on average. Taking into account the simplicity of our model, this can still be considered as consistent with observations: The horizontal and the vertical resolution of the model are relatively coarse compared to the spatial scale of fronts, eddies, and jet streams in the ACC, which are crucial for its dynamics. As a result, the average speed of the ACC is only roughly 4.4 cm s^{-1} in our model. Consequently, the timescale of the variability is increased in the LSG model.

Another difference between the ACW and the mode described in this paper lies in the characteristic zonal wavenumbers of the ocean and the atmospheric properties: WP describe the ACW as mainly a wavenumber two phenomenon. In our OGCM experiment a considerable fraction of the variance of the ocean response and the atmospheric forcing is distributed over the wavenumbers one, two, and three (Figure 5), which is similar to the wavenumber characteristic of the mode described by CBR. Since CBR used a completely different ocean model (OPYC3) at even higher resolution in their study, it is unlikely that these differences to observations can be attributed to deficiencies of the ocean models used. If we suppose that all modes under discussion represent the same physical phenomenon, it is more likely that the differences could be attributed either to the atmospheric model from which we derived the atmospheric forcing patterns and which is essentially the same as that used by CBR or to the short observational data record used by WP.

We found that the interannual variability in the Southern Ocean of our OGCM is to a large extent excited by random short-term atmospheric weather fluctuations. The anomalies are advected by the mean ocean circulation, which together with the dominant spatial scales of the atmospheric forcing determines the timescale of the ocean response. Because of the similarities between this stochastically excited mode and the variability described by CBR in a CGCM and by WP within observations, we suggest that the mechanism presented might be of some importance in the real Southern Ocean.

Appendix: AMIP

The Atmosphere Model Intercomparison Project (AMIP) is an international effort to undertake the systematic intercomparison and validation of the performance of numerous atmospheric general circulation models on seasonal and interannual timescales under as realistic conditions as possible. Particular emphasis is put on the simulation of the mean climate and the sequences of shorter climate states.

To enable intercomparison, all involved models simulate the same time period under comparable experimental conditions. As the AMIP test period, the decade 1979-1988 was selected. It includes the occurrence of the major ENSO event in 1982-1983. The period itself represents a compromise between the desire to simulate as long a period as possible and the increasing difficulties with the observational data as one steps back to earlier years.

All models are forced with the same observed global distributions of SST and sea ice, which are provided in terms of observed monthly averages on a $2° \times 2°$ spherical grid from which the appropriate interpolations can be made to force each model. A detailed description of the AMIP project can be found in the work of *Gates* [1992].

In the present paper we used monthly means of anomalous near-surface air temperatures and momentum, heat, and freshwater fluxes which were derived from an AMIP simulation with the ECHAM3-T42 AGCM [*Arpe et al.*, 1993].

Acknowledgments. We thank Eduardo Zorita, Reiner Schnur, and Chris Hughes for their valuable comments and the numerous discussions we had at the various stages of this paper. They helped to improve the paper significantly. This research was supported by grant BMBF-07VKVO1/1 of the German Bundesministerium für Bildung und Forschung.

References

Arakawa, A., and V.R. Lamb, Computational design of the basic processes of the UCLA general circulation model, *Methods Comput. Phys., 17*, 173-265, 1977.

Arpe, K., L. Bengtsson, and E. Roeckner, The impact of sea surface temperature anomalies on the variability of the atmospheric circulation in the ECHAM3 model, in *Research Activities in Atmospheric and Oceanic Modeling*, edited by G. Boer, pp. 7.18-7.20, *WMO Rep. 18*, World Meteorol. Organ., Geneva, 1993.

Basher, R.E., and C.S. Thompson, Relationship of air temperatures

In New Zealand to regional anomalies in sea surface temperature and atmospheric circulation, *Int. J. Climatol., 16*, 405-426, 1996.

Bonekamp, H., A. Sterl, and G. Komen, Interannual variability in the Southern Ocean from an OGCM forced by ECMWF reanalysis fluxes, *J. Geophys. Res.*, in press, 1999.

Christoph, M., T.P. Barnett, and E. Roeckner, The Antarctic circumpolar wave in a coupled ocean-atmosphere GCM, *J. Clim., 11*, 1659-1672, 1998.

Connolley, W.M., Variability in annual mean circulation in southern high latitudes, *Clim. Dyn., 13*, 745-756, 1997.

Frankignoul, C., and R. W. Reynolds, Testing a dynamical model for mid-latitude sea surface temperature anomalies, *J. Phys. Oceanogr., 13*, 1131-1145, 1983.

Gates, W.L., AMIP: The Atmospheric Model Intercomparison Project, *Bull. Am. Meteorol. Soc., 73*, 1962-1970, 1992.

Griffies, S.M., and E. Tziperman, A linear thermohaline oscillator driven by stochastic atmospheric forcing, *J. Clim., 8*, 2440-2453, 1995.

Hasselmann, K., Stochastic climate models, I, Theory, *Tellus, 28*, 473-485, 1976.

Hellerman, S., and M. Rosenstein, Normal monthly wind stress data over the world ocean with error estimates, *J. Phys. Oceanogr., 13*, 1093-1104, 1983.

Jacobs, G.A., and J.L. Mitchell, Ocean circulation variations associated with the Antarctic, *Geophys. Res. Lett., 23*, 2947-2950, 1996.

Lemke, P., E.W. Trinkl, and K. Hasselmann, Stochastic dynamic analysis of polar sea ice variability, *J. Phys. Oceanogr., 10*, 2100-2120, 1980.

Levitus, S., *Climatological Atlas of the World Ocean, NOAA Prof. Pap.*, Vol. 13, U.S. Gov. Print. Off., Washington, D.C., 1982.

Maier-Reimer, E., U. Mikolajewicz, and K. Hasselmann, Mean circulation of the Hamburg LSG OGCM and its sensitivity to the thermohaline surface forcing, *J. Phys. Oceanogr., 23*, 731-757, 1993.

Mikolajewicz, U., and E. Maier-Reimer, Mixed boundary conditions in ocean general circulation models and their influence on the stability of the models conveyor belt, *J. Geophys. Res., 99*, 22633-22644, 1994.

Mo, K.C., and G.H. White, Teleconnections in the Southern Hemisphere, *Mon. Weather Rev., 113*, 22-37, 1985.

Murphy, E.J., A. Clarke, C. Symon, and J. Priddle, Temporal variations in Antarctic sea-ice: Analysis of a long term fast-ice record from the South Orkney Islands, *Deep Sea Res. Part I, 42*, 1045-1062, 1995.

Peterson, R.G., and W. B. White, Slow oceanic teleconnections linking the Antarctic Circumpolar Wave with the tropical El Niño-Southern Oscillation, *J. Geophys. Res., 103*, 24573-24583, 1998.

Pratt, R.W., The interpretation of space time spectral quantities, *J. Atmos. Sci., 32*, 1283-1300, 1976.

Qiu, B., and F.F. Jin, Antarctic circumpolar waves: An indication of ocean-atmosphere coupling in the extratropics, *Geophys. Res. Lett., 24*, 2585-2588, 1997.

Roeckner, E., et al., Simulation of the present-day climate with the ECHAM model: Impact of model physics and resolution, *MPI Rep. 93*, 171 pp., Max-Planck-Inst. für Meteorol., Hamburg, Germany, 1992.

Rowell, D.P., Assessing potential seasonal predictability with an ensemble of multi-decadal GCM simulations, *J. Clim., 11*, 109-120, 1998.

Saravanan, R., and J.C. McWilliams, Advective ocean-atmosphere interaction: An analytical stochastic model with implications for decadal variability, *J. Clim., 11*, 165-188, 1998.

Schmitz, W.J., Jr., On the interbasin scale thermohaline circulation, *Rev. Geophys., 33*, 151-173, 1995.

Schnur, R., Baroklin instabile Wellen der Atmosphäre: Empirisch abgeleitete Moden im Vergleich zu quasi-geostrophischer Theorie, Ph.D. thesis, 70 pp., Univ. of Hamburg, Hamburg, Germany, 1993.

Schnur, R., G. Schmitz, N. Grieger, and H. von Storch, Normal modes of the atmosphere as estimated by Principal Oscillation Patterns and derived from quasi-geostrophic theory, *J. Atmos. Sci., 50*, 2386-2400, 1993.

UNESCO, Tenth report of the joint panel on oceanographic tables and standards, *UNESCO Tech. Pap. Mar. Sci., 36*, 25 pp., 1981.

von Storch, H., and F. W. Zwiers, *Statistical Analysis in Climate Research*, pp. 251-260, Cambridge Univ. Press, New York, 1999.

von Storch, H., G. Bürger, R. Schnur, and J.S. von Storch, Principal Oscillation Patterns: A review, *J. Clim., 8*, 377-400, 1995.

White, W.B., and R.G. Peterson, An Antarctic Circumpolar Wave in surface pressure, wind, temperature, and sea-ice extent, *Nature, 380*, 699-702, 1996.

Woodruff, S.D., R.J. Slutz, R.L. Jenne, and P.M. Steurer, A comprehensive ocean-atmosphere data set, *Bull. Am. Meteorol. Soc., 68*, 1239-1250, 1987.

Xu, J.S., H. von Storch, and H. van Loon, The performance of four spectral GCMs in the southern hemisphere: The January and July climatology and the semi-annual wave, *J. Clim., 3*, 54-70, 1990.

S. S. Drijfhout and A.Sterl, Koninklijk Nederlands Meteorologisch Instituut, Postbus 201, NL-3730 De Bilt, The Netherlands. (drijfhou@knmi.nl; sterl@knmi.nl)

U. Mikolajewicz, Max-Planck-Institut für Meteorologie, Bundesstrasse 55, D-20146 Hamburg, Germany. (mikolajewicz@dkrz.de)

R. Weisse, GKSS-Forschungszentrum Geesthacht, Institut für Gewässerphysik, Max-Planck-Strasse 1, D-21502 Geesthacht, Germany. (weisse@gkss.de)

(Received September 9, 1997; revised December 21, 1998; accepted February 8, 1999.)